Geophys. J. Int. (2003) **153,** 658–674

Holocene faulting and earthquake recurrence along the Serghaya branch of the Dead Sea fault system in Syria and Lebanon

Francisco Gomez,[1] Mustapha Meghraoui,[2] Abdul Nasser Darkal,[3] Fouad Hijazi,[4] Michel Mouty,[4] Youssef Suleiman,[4] Reda Sbeinati,[5] Ryad Darawcheh,[5] Riad Al-Ghazzi[4] and Muawia Barazangi[1]

[1]*Institute for the Study of the Continents, Snee Hall, Cornell University, Ithaca,* NY 14853, *USA. E-mail: fgomez@geology.cornell.edu*
[2]*EOST, Institut de Physique du Globe,* UMR 7516, *Strasbourg, France*
[3]*Department of Geology, Damascus University, Damascus, Syria*
[4]*Higher Institute of Applied Sciences and Technology, Damascus, Syria*
[5]*Department of Geology, Syrian Atomic Energy Commission, Damascus, Syria*

Accepted 2003 January 4. Received 2002 November 25; in original form 2002 July 24

SUMMARY

The Serghaya fault, located approximately along the Syrian–Lebanese border, is a prominent structure within the 200 km restraining bend in the left-lateral Dead Sea fault system. This study documents palaeoseismic and geomorphic expressions of Holocene movements on the Serghaya fault based on trench excavations and radiocarbon dates. Trenches were excavated across and parallel to a 4.5 m fault scarp where Late Pleistocene sediments are faulted against Holocene alluvium and colluvium. Locally oblique slip on the Serghaya fault has produced a sequence of fault-derived colluvial wedges that distinguishes individual palaeoseismic events. In addition, the trench excavations also depict a sequence of buried and displaced channels. Our palaeoseismic study reveals evidence for five surface-rupturing events within the past ~6500 yr. The last event involved 2–2.5 m of primarily left-lateral displacement and may correspond to one of two historically documented earthquakes during the 18th century (in 1705 and 1759). The displaced channels provide an estimated slip rate of approximately 1.4 ± 0.2 mm yr^{-1} during the Holocene. The chronological relationships between the colluvial wedges and faulted channels demonstrate an average left-lateral displacement of about 2 m per event, suggesting that such events correspond to earthquakes of $M \gtrsim 7$ with a mean return time of about 1300 yr. These results demonstrate that the Serghaya fault may present a previously overlooked earthquake hazard for populations in the vicinity of the AntiLebanon Mountains, including the cities of Damascus and Beirut. In a regional context, the inferred slip rate along the Serghaya fault accounts for about 25 per cent of the total expected motion of Arabia relative to Africa along the Dead Sea fault system. The fact that the Serghaya fault accounts for only a fraction of the expected plate motion implies that the remaining strike-slip and shortening must be accommodated by other active fault branches within the large restraining bend of the Dead Sea fault system. These results contradict suggestions that the northern Dead Sea fault system in Lebanon and Syria is presently inactive as a result of an evolving regional stress field in the eastern Mediterranean region.

Key words: Dead Sea fault, earthquakes, Lebanon, slip rate, Syria.

1 INTRODUCTION

Spanning nearly 1000 km from the Gulf of Aqaba in the south to the Taurus Mountains in southern Turkey, the Dead Sea fault system (DSFS) ranks among the largest strike-slip fault systems in the world and represents a key element of the eastern Mediterranean tectonic framework. The DSFS is the left-lateral transform boundary between the Arabian and African plates and accommodates their differential convergence relative to Eurasia (e.g. Freund *et al.* 1970; Ben Menahem *et al.* 1976). However, recent debates concerning the slip rate and kinematics of the DSFS, especially the activity of the northern ~500 km of the DSFS in Lebanon and Syria (e.g. Girdler 1990; Butler *et al.* 1997), attest to the limited understanding of the DSFS as an active and seismogenic system.

The general structure of the left-lateral DSFS consists of two relatively simple northern and southern sections, joined by a ~200 km

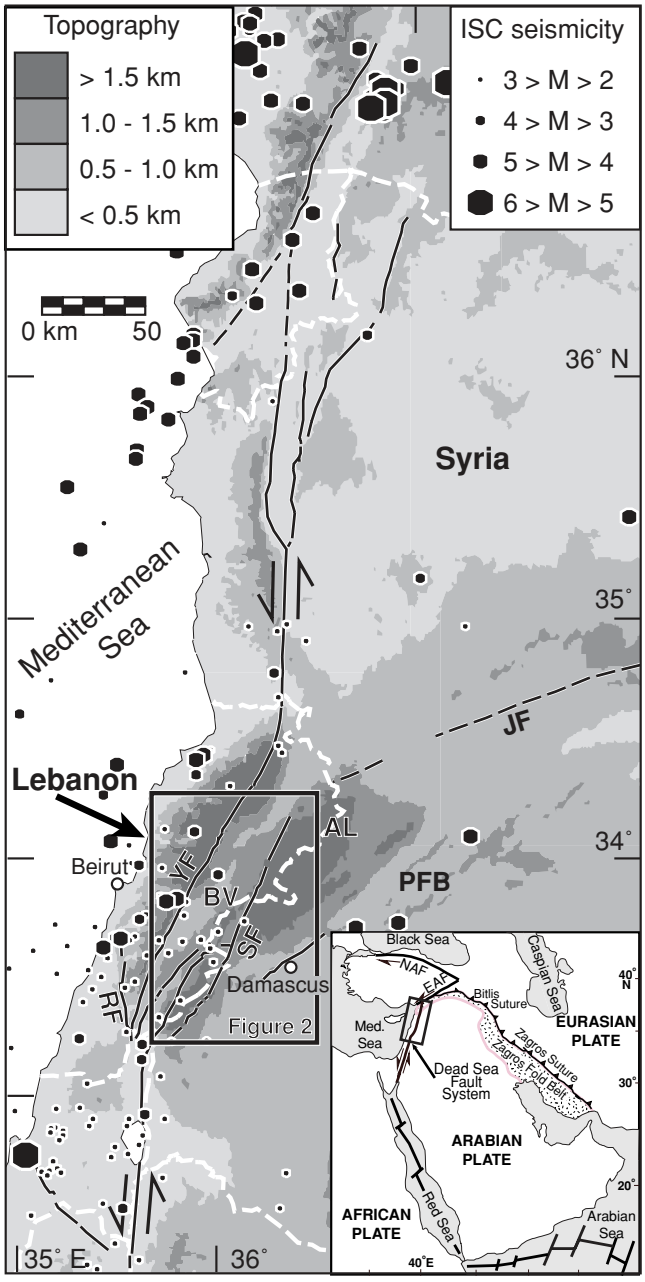

Figure 1. Simplified topography and tectonic map of the northern Dead Sea fault system. Tectonic and physiographic features: SF = Serghaya fault, YF = Yammouneh fault, RF = Roum fault, JF = Jhar fault, AL = AntiLebanon Mountains, PFB = Palmyride fold belt, BV = Bekaa Valley. The inset depicts the plate tectonic context of the Dead Sea fault system. Faults are simplified from Dubertret (1962).

long restraining bend located mostly in Lebanon (see Fig. 1; Garfunkel *et al.* 1981; Quennell 1984; Beydoun 1999). Within this restraining bend, the fault system comprises several distinct fault branches (e.g. Walley 1988). An understanding of which structures are active, along with their kinematics, is essential to unravelling the nature and tectonic evolution of this part of the plate boundary and how it links the structurally simpler sections of the DSFS to the north and south.

Another motivation for studying active tectonics of the DSFS is a better understanding of the regional earthquake hazard in the eastern Mediterranean. The DSFS, in particular, presents a special opportunity to integrate several millennia of historical records of large earthquakes with palaeoseismic methods in order to understand the processes of earthquake recurrence in the plate boundary deformation. Historical accounts testify to large and devastating earthquakes along the DSFS over the past several millennia (e.g. Poirier & Taher 1980; Ambraseys & Barazangi 1989; Ambraseys *et al.* 1994; Amiran *et al.* 1994; Darawcheh *et al.* 2000; Sbeinati *et al.* 2002).

For the central and northern DSFS, these historical records contrast with instrumental records of seismicity during the past century depicting little earthquake activity (e.g. Ambraseys & Jackson 1998). This apparent behaviour of seismic quiescence punctuated by large earthquakes underscores the need for geological studies of past earthquakes (i.e. palaeoseismology and tectonic geomorphology) to understand the patterns of large earthquake recurrence along this plate boundary. During the past decade, palaeoseismic investigations along the southern DSFS have proven successful in identifying surface ruptures associated with historical earthquakes (e.g. Ellenblum *et al.* 1998; Ken-Tor *et al.* 2001), as well as documenting evidence for long-term earthquake behaviour such as temporal clustering (e.g. El-Isa & Mustafa 1986; Marco *et al.* 1996; Zilberman *et al.* 2000). Aside from one recent study at the site of a faulted Hellenistic or Roman aqueduct in Syria (Meghraoui *et al.* 2003), similar studies are, in general, lacking for the central and northern DSFS in Lebanon and Syria (i.e. from the restraining bend northward). In addition to earthquake recurrence histories, fundamental kinematic parameters such as rates of fault slip are not well documented. Hence, the DSFS presents a poorly understood earthquake hazard for the surrounding populations, particularly in the central and northern sections. In the case of the restraining bend, the relative activity of different active branches will have implications for earthquake hazard assessment, particularly if concepts such as stress triggering and fault interactions are considered (e.g. Stein *et al.* 1997; Mohamad *et al.* 2000).

This study examines the Serghaya fault, a branch of the DSFS within the restraining bend that, until recently, has been generally regarded as inactive since the Pliocene (e.g. Walley 1988; Girdler 1990; Butler *et al.* 1997). This study presents detailed observations and analyses that build upon our previously reported reconnaissance work in the region (Gomez *et al.* 2001). These new results demonstrate that the Serghaya fault has important implications in terms of regional tectonics and earthquake hazard. Palaeoseismic and geomorphic evidence demonstrates a record of Holocene earthquakes and provides a Holocene slip rate for this fault branch. After discussing the implications for the regional earthquake hazard, these results are placed within the context of present-day regional tectonics of the DSFS.

1.1 Regional tectonic and seismotectonic setting

The present-day relative motion between Arabia and Africa is estimated to be 4–8 mm yr^{-1}, based on plate tectonic models (e.g. Joffe & Garfunkel 1987; Jestin *et al.* 1994) and recent GPS observations (e.g. McClusky *et al.* 2000, 2003). This is consistent with geological estimates of Quaternary slip rates for the southern DSFS (e.g. Garfunkel *et al.* 1981; Klinger *et al.* 2000a), as well as an estimated slip rate, averaged over ~2000 yr, from the aforementioned faulted aqueduct in Syria (Meghraoui *et al.* 2003). Interestingly, almost all models of instantaneous (i.e. present-day) plate motions predict a general northward increase in the rates of slip along the DSFS, as well as increasing the component of relative convergence between the Arabian and African plates across the DSFS. This assumes

that all of the relative plate motion is accommodated by the DSFS. The present episode of tectonic activity of the DSFS is believed to have initiated during the end of the Miocene or early Pliocene (e.g. Hempton 1987).

Available seismotectonic observations, although limited, are consistent with the general model of a continental transform system. The kinematics of the large Gulf of Aqaba earthquake in 1995 ($M \sim 7.3$) demonstrated predominantly left-lateral motion along the southern DSFS (Pinar & Turkelli 1997; Klinger *et al.* 1999). The paucity of large, instrumentally recorded earthquakes has precluded accurate assessment of seismic moment release along the plate boundary (e.g. Jackson & McKenzie 1988). However, some have suggested 6–10 mm yr^{-1} of slip by inferring seismic moment and other parameters of large, historically documented earthquakes (e.g. Westaway 1994). The morphological expression of the DSFS from remotely sensed imagery also shows a general spatial correspondence with seismicity patterns (e.g. Al Ghazzi 1992).

The 200 km long northeast–southwest striking restraining bend encompasses the Mt Lebanon and AntiLebanon ranges. At the southern end of this restraining bend, the relatively simple trace of the southern DSFS branches into several distinct fault splays, including the Yammouneh, Serghaya, Rachaya, Hasbaya and Roum faults (Fig. 1) (e.g. Walley 1988; Heimann & Ron 1993). Of all of these fault branches, the Yammouneh fault is the only throughgoing structure that connects the northern and southern sections of the DSFS.

Adjacent to the restraining bend, the Palmyride fold belt is another regionally prominent tectonic element (Fig. 1). This Cenozoic fold belt corresponds to a Late Palaeozoic–Early Mesozoic (Neo-Tethyan) rift basin that was tectonically inverted during the Cenozoic (e.g. Chaimov *et al.* 1990). Scattered seismicity suggests that the Palmyride region is still tectonically active (e.g. Chaimov *et al.* 1990; Brew *et al.* 2001). Hence, the Palmyrides represent some internal deformation of the Arabian plate that might have some kinematic relationship with the plate boundary deformation of the DSFS.

1.2 Serghaya fault and Zebadani valley

Branching from the southern DSFS in the Golan Heights, the Serghaya fault can be traced approximately 125 km through the AntiLebanon Mountains to the eastern edge of the Bekaa Valley (Fig. 2). A detailed map of the Serghaya fault zone (Fig. 2) has resulted from the analysis of remote sensing imagery (satellite imagery and aerial photos), a high-resolution (20 m pixel) digital elevation model (DEM), information from published geological maps (e.g. Dubertret 1955), and ground-truth from field investigations. Fig. 2 also depicts the morphology of the region using the DEM to generate a shaded relief image. The gross geomorphic expressions of the Serghaya fault include the alignment of linear valleys and large stream valley deflections. Almost all valleys show clear leftward deflections implying long-term, tectonic control of the landscape. Furthermore, left steps in the fault zone correspond to the elongate basins, suggesting these are pull-apart basins.

Along the southern half of the Serghaya fault, the uplift of the Mt Hermon block in the AntiLebanon Mountains forms within an apparent strike-slip duplex comprising the Serghaya and Rachaya faults (Fig. 2). This interpretation of a crustal sliver trapped between two strike-slip faults is consistent with reported vertical-axis rotations of the Mt Hermon region observed with palaeomagnetic data (e.g. Ron 1987; Heimann & Ron 1993). Field evidence for Quaternary strike-slip faulting along the Serghaya fault is observed as far north as the village of Aarsal, near the edge of the Bekaa Valley (Fig. 2). North of this point, the trace of the Serghaya fault is obscure. Existing geological maps and overhead imagery depict neither geomorphic nor structural indications to suggest that the northern Serghaya fault reconnects with the transform boundary (Fig. 2). Such a linkage would be expected to involve local extension and subsidence (a leftward step in a left-lateral fault system), and these phenomena are not apparent.

Although the Serghaya fault primarily traces through the Mesozoic carbonate bedrock of the AntiLebanon Mountains, the fault occasionally passes through Quaternary basins, providing an opportunity to observe the expressions of recent fault movements. In the Zebadani Valley of Syria (Fig. 2), the focus of this study, the Serghaya fault bounds the eastern side of the valley. The stereonet in Fig. 3 depicts the fault planes and associated striations measured in faulted Late Pleistocene lake sediments in the southern Zebadani Valley. Shear indicators (e.g. slickenside striations and tool marks) demonstrate predominantly left-lateral slip. Rakes of 10°–20° are observed on subvertical fault planes, implying a ratio of strike-slip to dip-slip between 4:1 and 5:1. A 4.0–4.5 m fault scarp results from the oblique fault slip along this portion of the Serghaya fault. Locally, the fault scarp preserves a free face, attesting to recent fault movement. The free face heights suggest approximately 0.5 m of dip slip for the last episodic movement (Gomez *et al.* 2001).

Small hillslope drainage deflections also coincide with the fault scarp (Fig. 4). Many of these deflections have been measured and interpreted as true fault displacements (Gomez *et al.* 2001). All of these small drainages depict minimum deflections of 1.9–2.5 m, as well as larger, composite stream deflections (Fig. 3). The proportion of strike-slip to dip-slip suggested by the stream deflections and scarp free faces, respectively, is consistent with the fault kinematic indicators (stereonet in Fig. 3). Hence, these recent movements are most likely to be contemporaneous.

One colluvial wedge corresponds to the remnant of the free face, suggesting that the free face represents only one palaeoseismic event (e.g. McCalpin 1996). Radiocarbon dating has constrained this paleoseismic indicator within the past 300 yr (Gomez *et al.* 2001). Hence, the free faces and minimum drainage displacements are probably the expressions of the last surface rupturing earthquake, and this event may correspond to one of two well-documented earthquakes that strongly affected the AntiLebanon Mountains and surrounding regions in the early and mid 18th century (i.e. in 1705 and 1759; see Table 1). The recent timing of this event is also supported by the preservation of a fault scarp free face in Late Pleistocene lake sediments.

2 PALAEOSEISMIC STUDY: METHODS AND RESULTS

The presence of an active fault with an apparent coseismic displacement during recent history motivated our effort to extend the record of past earthquakes and their associated displacements back through the Holocene. The evidence of a prominent, young fault scarp and consistent left-lateral stream offsets, along with lacustrine and alluvial deposits, suggested that the southern Zebadani valley might be a promising site for palaeoseismic investigation. Our study focused on a site near the village of Tekieh (see Figs 3, 5 and 6) where the fault juxtaposes recent alluvium against Late Pleistocene lacustrine sediments. Microtopographic mapping and analysis was combined with a trench excavation in order to document the earthquake history of the Serghaya fault.

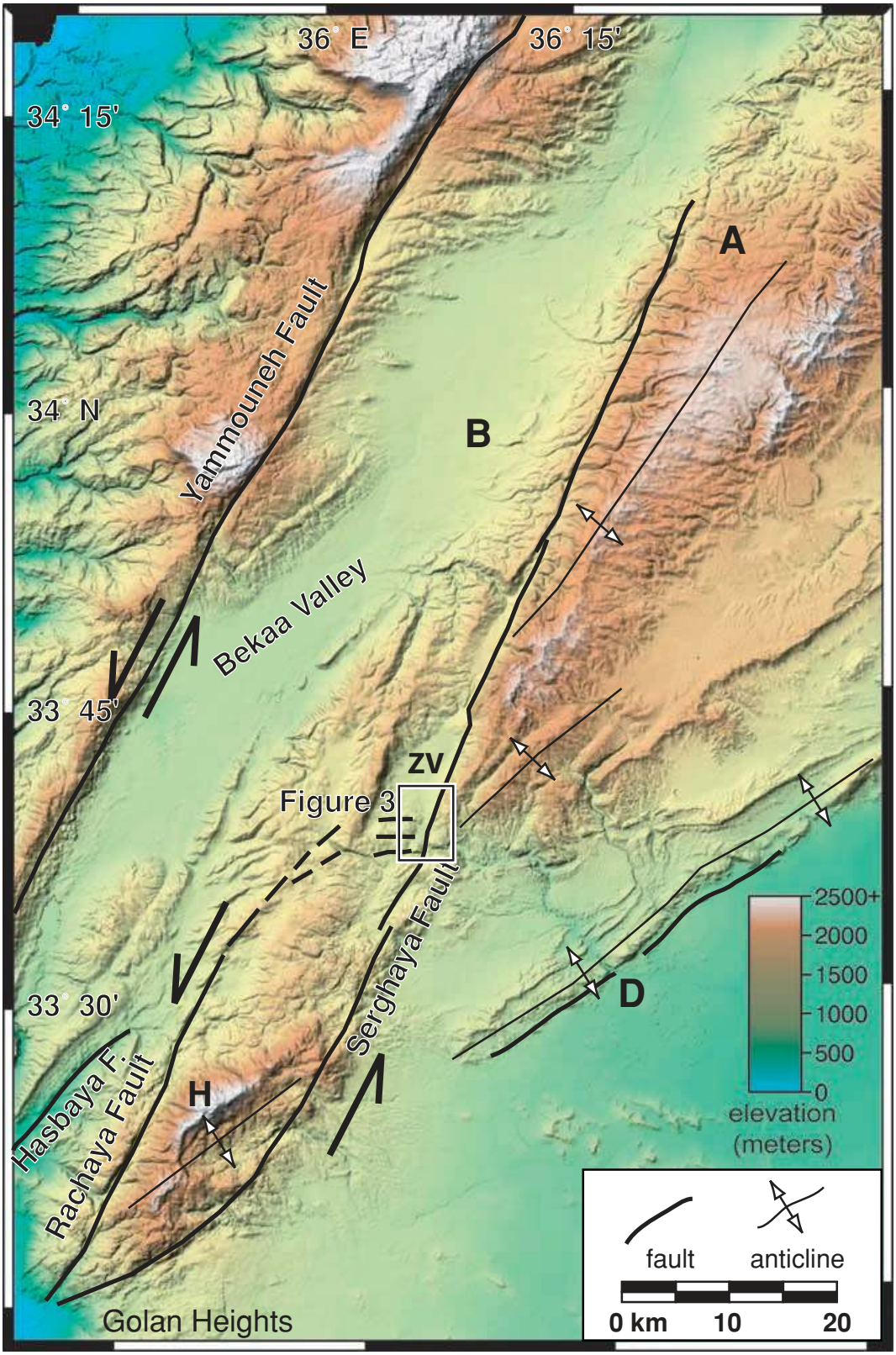

Figure 2. Shaded relief image depicting the gross morphology of the Serghaya fault. Faults and the main anticlinal hinges are shown. Geographic features: ZV = Zebadani Valley, H = Mt Hermon, D = Damascus, B = Baalbek, A = Aarsal. See Fig. 1 for location.

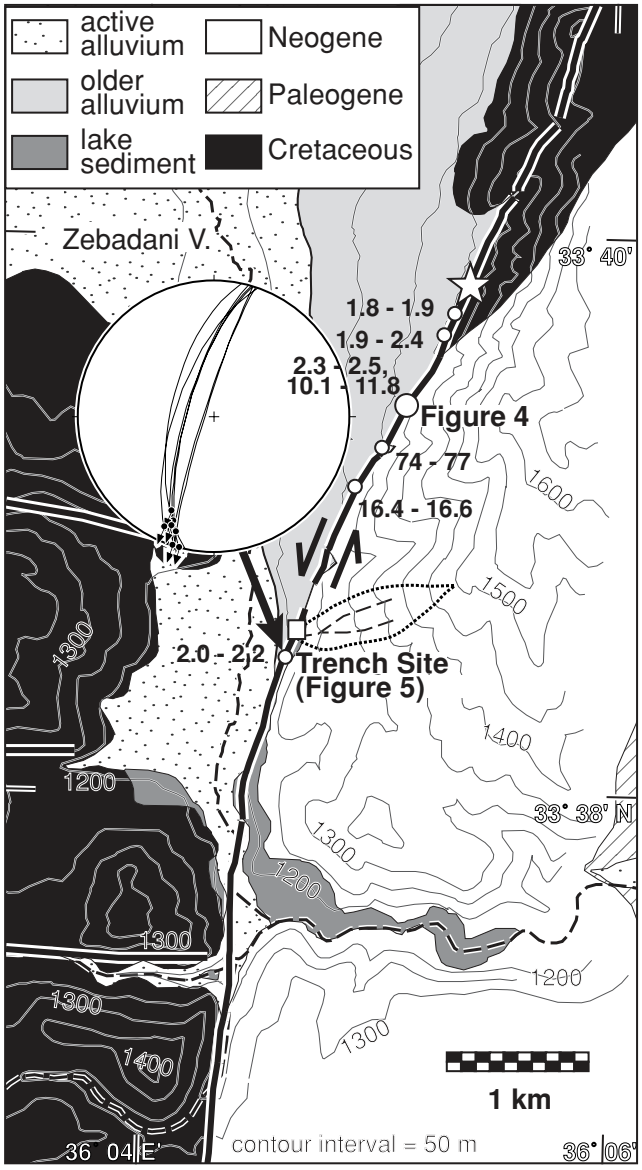

Figure 3. Geology of the southern Zebadani Valley (Syria). See Fig. 2 for location. Stereonet depicts fault planes and associated striations from faulted Late Pleistocene lake sediments. The dotted line depicts the catchment for the hillslope drainage at the trench site (white square). The white star denotes the excavation of the upper colluvial wedge described in Gomez *et al.* (2001). White discs denote small drainage deflections (values in metres), including the example shown in Fig. 4. Topographic contour interval = 50 m.

2.1 Local morphology

The Serghaya fault is represented by a composite fault scarp ~4.0–4.5 m high and comprising the boundary between the mountain front and the Late Quaternary alluvial apron (Fig. 6). As shown in the topographic profile (Fig. 5b), the lower alluvial surface appears to correspond to the bevelled bedrock in the upper surface. About 150 m to the south can be found some of the free faces reported by Gomez *et al.* (2001).

The up-thrown eastern block of the fault comprises Late Quaternary lacustrine sediments (calcareous silt and gravel) and Pliocene–Quaternary conglomerates (Fig. 5). Radiocarbon dating of a charcoal fragment from a roadcut exposure of the lacustrine sediments about 0.5 km to the south yielded a radiocarbon age of 44.6 kyr BP (sample LS-1 in Table 2).

At the trench site, a hillslope drainage with a small catchment area of approximately 0.25 km^2 exits the mountain front (Fig. 3). This ephemeral stream feeds a young alluvial fan that attains up to about 1 m of relief above the surface of the older alluvial apron (Fig. 5). Although today partially truncated on the north side by an orchard, the northern limit of the younger fan was mapped from aerial photos dating to 1983.

Emerging from the mouth of the drainage at the fault scarp, the active, ephemeral streambed deflects southward (i.e. left-lateral) approximately 2 m (Fig. 5). This deflection is consistent with the minimum deflections observed in other small drainages in the southern Zebadani Valley (Fig. 3; Gomez *et al.* 2001). Hence, we interpret this deflection as a displacement corresponding to the last surface-rupturing earthquake in the early or mid 18th century.

2.2 Palaeoseismic trenching

The system of three trenches shown in Figs 5 and 6 was designed to take advantage of both the vertical and lateral components of the locally oblique fault slip. The trenches were excavated using a backhoe, and the walls were subsequently cleaned by hand. A 1 m grid facilitated the careful logging of all six trench walls (three trenches with two walls each) at a scale of 1:20. Within the study site, we mapped the precise positions of the trenches with respect to the present-day stream channel and fault scarp using a total station.

Trench 1 spanned approximately 8 m across the fault zone and exposed the Late Pleistocene lacustrine deposits and the alluvial sediments. This trench was excavated to depths from 2.5 to 4 m and provided a view of the relationships between faulting and different colluvial/alluvial deposits.

Trenches 2 and 3 were excavated 2–2.5 m deep, parallel to the fault scarp (NNE–SSW) from the mouth of the drainage southward across the alluvial fan. These fault-parallel trenches, located 4 and 7 m from the fault, were excavated in order to explore for indications of lateral displacement. Furthermore, the intersection of Trenches 1 and 2 provided possible stratigraphic ties within the excavation site.

The results presented below reflect all six trench logs. However, for the sake of simplicity, only two trench logs are shown: one wall of the trench crossing the fault (Trench 1; Figs 7 and 8), and one wall of the fault-parallel trench nearer the fault scarp (Trench 2; Figs 9 and 10).

2.3 Radiocarbon dating

The critical age control in this study relied upon radiocarbon dating of buried organic material (Table 2). Samples of detrital charcoal, buried wood and buried seeds were collected from the trench walls, as well as a sample of charcoal collected from the lacustrine sediments approximately 0.5 km to the south of the trench site (see Table 2). In addition, bulk sediment samples were collected from stratigraphic units more than 1 m below the surface. Small samples were dated using accelerator mass spectrometry (AMS), and bulk samples from buried soils were crushed, slurried and sieved prior to chemical pretreatment and dating by decay counting.

Some of the samples, particularly those from shallow levels in the trenches, show evidence of probable contamination. These samples are evident with ^{14}C concentrations greater than 100 per cent of the modern value in Table 1. These samples were typically very small and collected from the uppermost colluvial deposit. We interpret

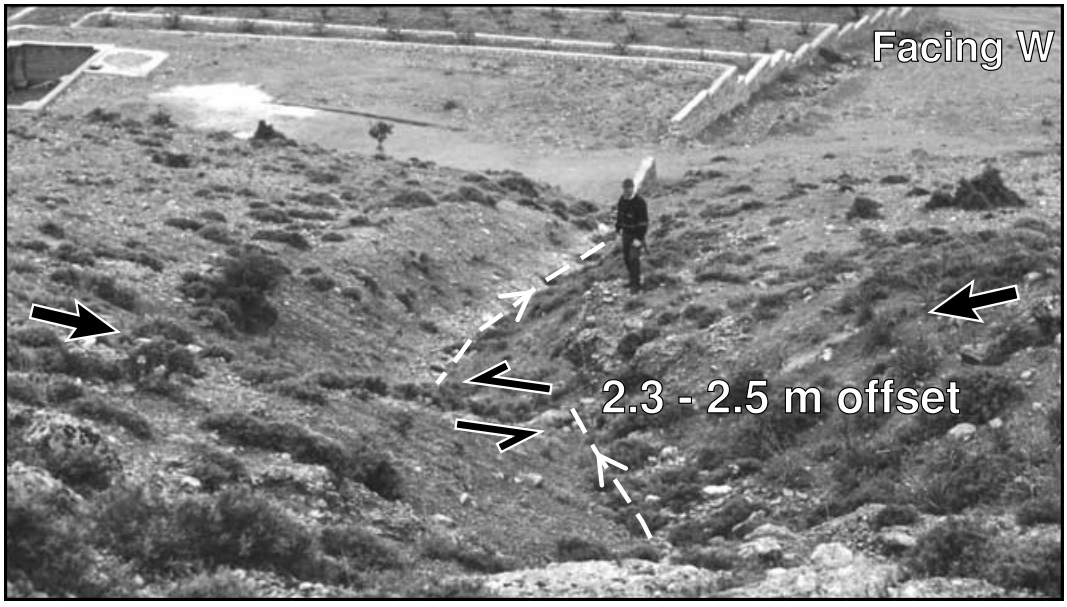

Figure 4. An example of a small, displaced drainage crossing the Serghaya fault. The minimum offset is 2.3–2.5 m. The view is facing west; see Fig. 3 for location.

Table 1. Large historical earthquakes in western Syria and Lebanon (32.5°–35.5°N).

Year	*M*	Affected areas (in order of decreasing intensity)
198 BC	?	Lebanese coast, southern Syria
115 AD	?	Northwest Syria
303 AD	∼7.0	Lebanese coast, southern Syria
551 AD	7.0–7.5	Lebanese coast
749 AD	7.0–7.5	Southern Bekaa Valley, southern Syria
859 AD	7.0–7.5	Northwest Syria
991 AD	7.0–7.5	Bekaa Valley, AntiLebanon
1063 AD	∼7.0	Northern Lebanese coast, Syrian coast
1157 AD	7.0–7.5	Northwest Syria, Ghab Valley
1170 AD	>7.5	Northern Lebanon, Syrian coast
1202 AD	>7.5	Mt Lebanon, Bekaa Valley, Hula Basin, Lebanese–Syrian coast
1705 AD	∼7.0	AntiLebanon, Zabadani and Bekaa Valleys, Damascus, northern Lebanese coast
1759 AD	∼7.4	Bekaa Valley, AntiLebanon, Golan Heights, Mt Lebanon, Damascus
1837 AD	7.0–7.5	Western Lebanon, southern Bekaa Valley, Hula Basin

Data from Poirier & Taher (1980), Ambraseys & Barazangi (1989), Ambraseys & White (1997), Ambraseys & Jackson (1998) and Sbeinati *et al.* (2003).

these as probable contamination based on previous information concerning the uppermost colluvial deposit. Previous dating of relatively intact exposures of the uppermost colluvial wedge (which we correlate with the uppermost colluvial deposit in this study) was reported by Gomez *et al.* (2001) as radiocarbon 'modern'. Furthermore, in this study area, the uppermost colluvial wedge has been severely truncated by agricultural activity. These samples were collected just below the plow zone at depths of 0.2 m. Hence, there seems to be considerable potential for contamination of these small samples by post-bomb carbon.

The quality of the other reported charcoal samples (from deeper levels in the trenches) is generally good—these were typically larger samples (>120 μM of graphitized carbon). However, both of the bulk sediment samples yielded very small amounts of organic carbon (<0.5 g) and required extended counting.

We calibrated radiocarbon ages to calendar dates with the correction curve of Stuiver *et al.* (1998) using the OxCal program (Bronk Ramsey 1998), and these calibrated ages are reported as ranges of dates representing the probability density function at the 95 per cent (2σ) confidence limits (Table 2). In some cases, the calibrated age ranges were further constrained by applying rules of superposition and Bayesian analysis (e.g. Biasi & Weldon 1994; Bronk Ramsey 1998). This was particularly helpful in assigning probable ages to the base of the earthquake sequence where there is sufficient age control (i.e. relating Channel C3 incision and fill to Wedge 2, see below).

2.4 Trench 1: colluvial wedge stratigraphy

Across the fault zone, Trench 1 exposed a stratigraphy of Late Pleistocene lacustrine marl and sandy gravel in the up-thrown block and reddish brown to yellowish alluvium and colluvium on the down-thrown (western) side of the fault. The photomosaic of the northern trench wall in Fig. 7 and the associated trench log in Fig. 8 show the abrupt fault contact between the lacustrine sediments and the younger alluvium. The fault zone is 3–4 m wide, as revealed by shear fabrics in the silt and clay and by alignments of elongate clasts in the matrix-supported alluvium.

Undifferentiated reddish brown alluvium (unit a) characterizes much of the lower stratigraphy (Fig. 8). This deposit consists of gravel, sand, and occasional cobble supported by a clay matrix. This stratigraphic unit appears to correspond to the alluvial apron flanking the mountain front. Locally, it is buried beneath the younger alluvial fan deposit, and adjacent to the fault scarp, it has been buried beneath up to 1.5 m of scarp-derived colluvium. A bulk soil sample from the top of unit a (i.e. just below colluvial deposit W2) yielded an age of 5280 ± 230 BP. Applying Bayesian methods to the radiocarbon calibration (Biasi & Weldon 1994)—specifically, knowing that the undifferentiated alluvium predates buried channels

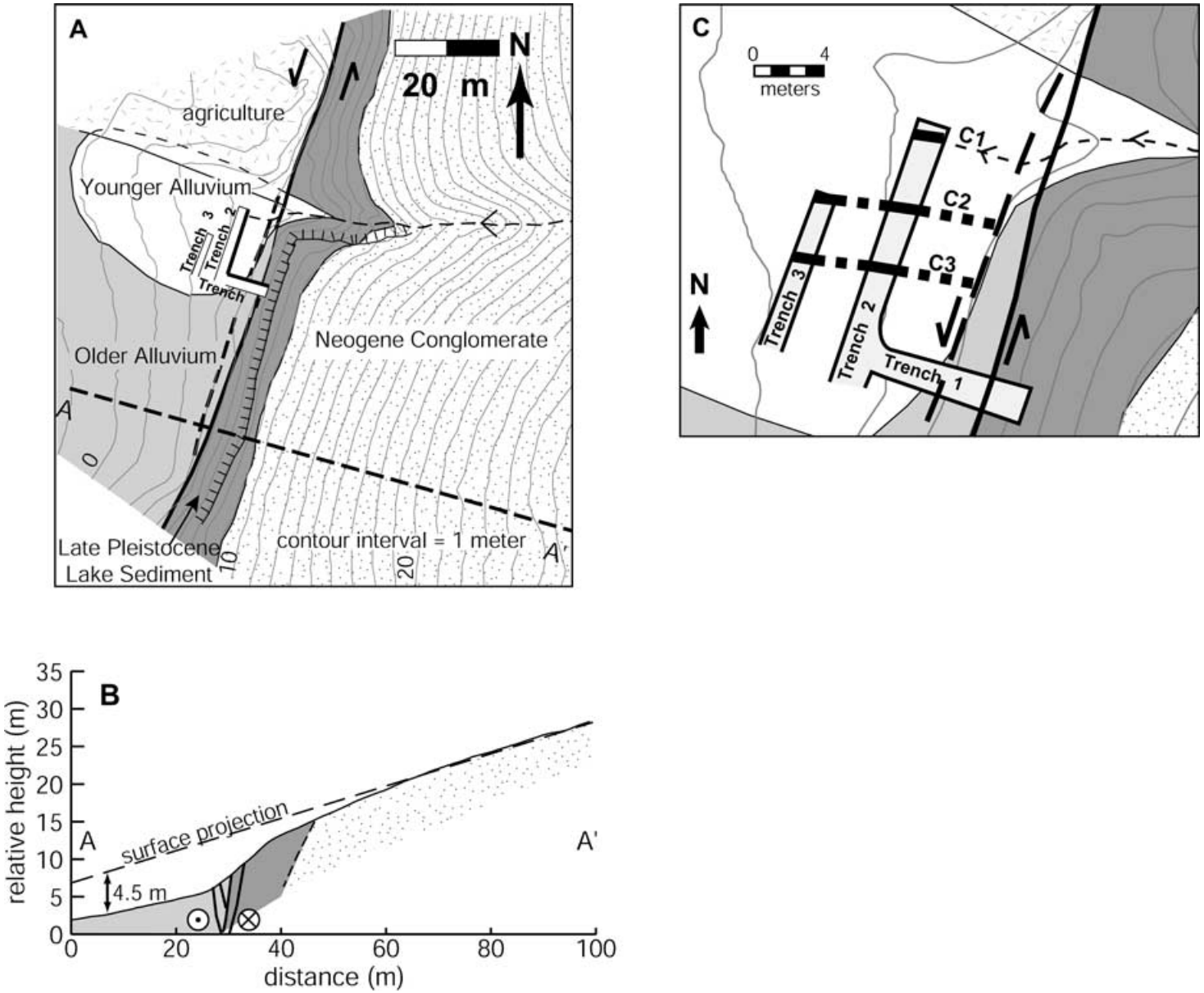

Figure 5. (a) Map of trench site. 1 m relative contours are based on mapping with a total station. See Fig. 3 for location. (b) Topographic profile and cross-section illustrating composite fault scarp approximately 4.5 m in height. (c) Enlarged map of the trench site depicting the positions of the present channel (C1) and the precise locations of the buried channels (C2 and C3). Solid black lines indicate where the buried channels were observed and dashed lines indicate where buried channels were inferred. The patterns are consistent with Fig. 5(a).

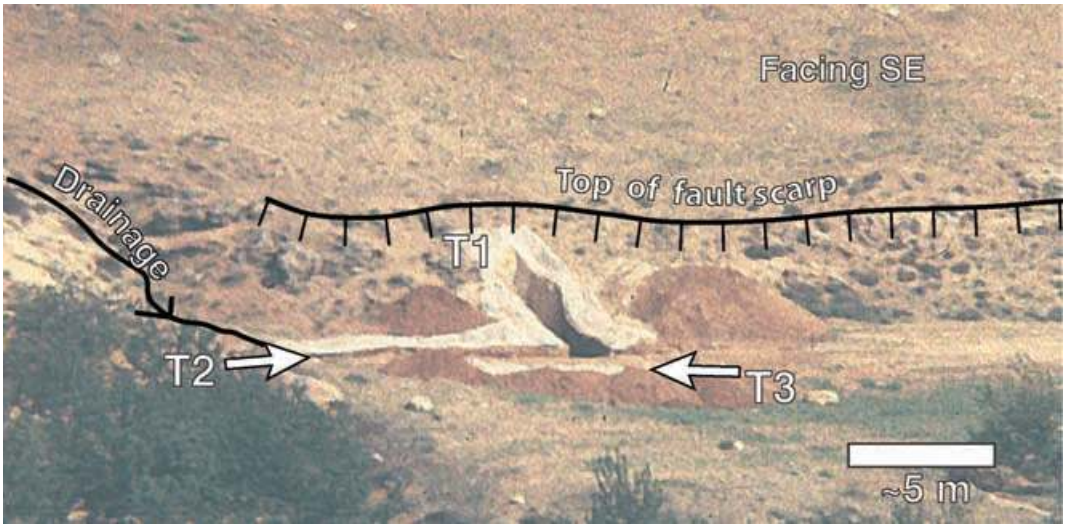

Figure 6. Photograph of the trench site facing SE. Note the position of the trench system relative to the fault scarp and the small drainage. See Fig. 3 for location.

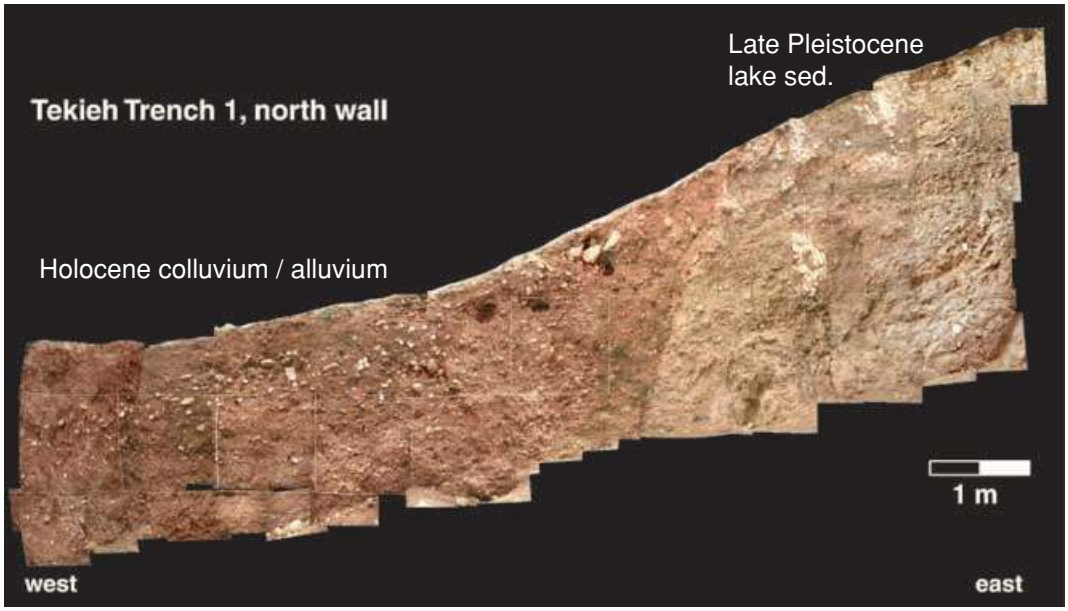

Figure 7. Photomosaic of the north wall of Trench 1.

incised into unit a (discussed below)—we calculate a calibrated age of 4720–4270 BC for the undifferentiated alluvium.

Colluvial 'wedge' deposits along fault scarps are important palaeoseismic indicators in cases where local fault movements involve repeated uplift (e.g. McCalpin 1996). In Trench 1, individual colluvial deposits are distinguished by pebbles and other larger clasts defining buried depositional surfaces. The colluvium consists of poorly sorted, matrix-supported clasts of Late Pliocene–Quaternary conglomerate and lacustrine marl, and the clasts are typically angular to subangular, suggesting proximal sources. The development of distinct soils in each colluvial wedge suggests long-term stability of the surface during the time between colluvial depositional events. These colluvial wedges are bounded on the up-thrown, eastern sides by buried scarps 20–40 cm in height. These scarps align with shear zones truncating the lower strata, implying that the buried scarps result from fault movements. Furthermore, some of these colluvial bodies are themselves truncated by subsequent faulting as indicated by shear fabrics and buried by younger colluvium.

In total, we distinguished five colluvial wedges above the undifferentiated alluvium (unit a), as well as one within. For this discussion, these are labelled in ascending order as Wedges 1 through 6 (Fig. 8). The colluvial wedges proved challenging for dating owing to a lack of sufficient organic material. Some of the samples show apparent contamination such as modern radiocarbon ages reported for samples from considerable depth. Dates from Wedges 6, 5 and 2 (corresponding to the uppermost, penultimate and earliest post-unit-a colluvium, respectively) were obtained.

At this site, the uppermost colluvial wedge (Wedge 6) was to be truncated by the plow zone—the thickness is minimal, and a plastic cigarette wrapper was found 25 cm below the surface, implying recent modification. The remnant of this wedge consisted of centimetre-size pebbles and gravel clasts of limestone and lake

Table 2. Radiocarbon dates of relevant samples from Trenches 1 and 2 and nearby areas.

Sample	Method	Material	Sampled layer	δ^{13}C per mil	Radiocarbon age years BP	2σ calibrated age range
LS-1	AMS	Charcoal	Quaternary lake sediment	−25.0	44 630 ± 1570	n/a
T1-02Nd	AMS	Charcoal	Colluvium, Wedge 5	−25.0	2060 ± 30	170 BC–20 AD
T1-09N	AMS	Seed	Colluvium, Wedge 6	−24.2	>Modern (122.8 ± 0.3 per cent)	Post 1950 AD
T1-04S	AMS	Seed	Colluvium, Wedge 6	−25.2	>Modern (111.4 ± 0.5 per cent)	Post 1950 AD
T1-15S	AMS	Seed	Silty sand below Wedge 6	−24.1	>Modern (125.8 ± 0.3 per cent)	Post 1950 AD
T2-05E	AMS	Charcoal	Sandy gravel, Channel 3	−26.0	5510 ± 80	4540BC–4160 BC
T1-03N	AMS	Charcoal	Silty sand below Wedge 6	(−25.0)	>Modern (103.9 ± 1.8 per cent)	Post 1650 AD
T2-10W	AMS	Charcoal	Sandy gravel, Channel 3	(−25.0)	5450 ± 140	4600 BC–3950 BC
T1-108S	AMS	Charcoal	Silty sand below Wedge 6	−27.3	>Modern (110.7 ± 0.5 per cent)	Post 1950 AD
T2-15E	AMS	Charcoal	Sandy gravel, Channel 1	−26.2	1354 ± 52	600 AD–780 AD
T2-101W	AMS	Charcoal	Sandy gravel, Channel 2	−25.4	3233 ± 57	1690 BC–1400 BC
T2-101 E	AMS	Charcoal	Sandy gravel, Channel 3	−25.6	5492 ± 57	4460 BC–4250 BC
T1-107S	AMS	Charcoal	Silty sand below Wedge 6	−27.7	>Modern (133.7 ± 0.5 per cent)	Post 1950 AD
T3-07E	AMS	Charcoal	Sandy gravel, Channel 3	−25.7	5540 ± 51	4500 BC–4250 BC
T1-110Nbk	CONV	Soil organics	Colluvium, Wedge 2	−25.7	4870 ± 160	4050 BC–3100 BC
T1-104Sbk	CONV	Soil organics	Undifferentiated alluvium	−24.7	5280 ± 230	4700 BC–3700 BC
T1-107Nbk	CONV	Soil organics	Soil below colluvium	−25.0	6590 ± 120	5730 BC–5320 BC

Dating methods are AMS (accelerator mass spectrometer) and conventional (i.e. decay counting). Samples have been calibrated with OxCal 3.5 by Bronk Ramsey using the data set of Stuiver *et al.* (1998). Radiocarbon ages of >modern are listed with the per cent Modern values. δ^{13}C values in parentheses indicate that the sample was too small for a δ^{13}C measurement and a value was assumed.

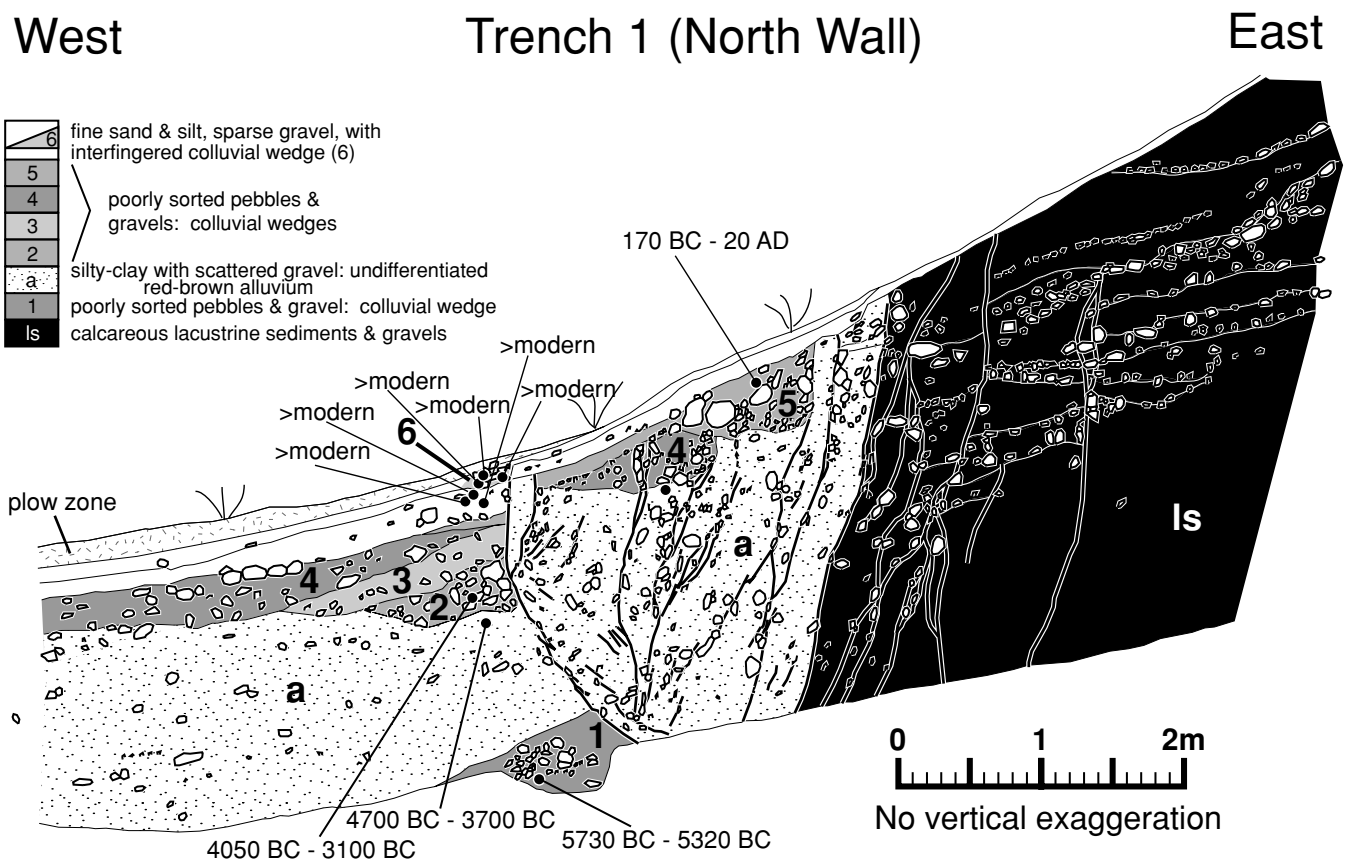

Figure 8. Trench log for the northern wall of Trench 1 (see Fig. 7), exposing colluvial wedges, undifferentiated alluvium and Late Pleistocene lake sediments. Calibrated radiocarbon ages are shown.

sediments. Dating of this wedge was difficult. From within Wedge 6, only small seeds were extracted yielding high concentrations of ^{14}C in excess of 100 per cent modern. These 'post-bomb' samples may, in fact, be very recently deposited, particularly since the top of Wedge 6 has been truncated by modern cultivation (Fig. 8). One charcoal fragment from the sand immediately below Wedge 6 (sample T1-03N with 103.9 ± 1.8 per cent modern) yielded a calendar age of 1650 AD to present. Owing to its small size (<27 μM of

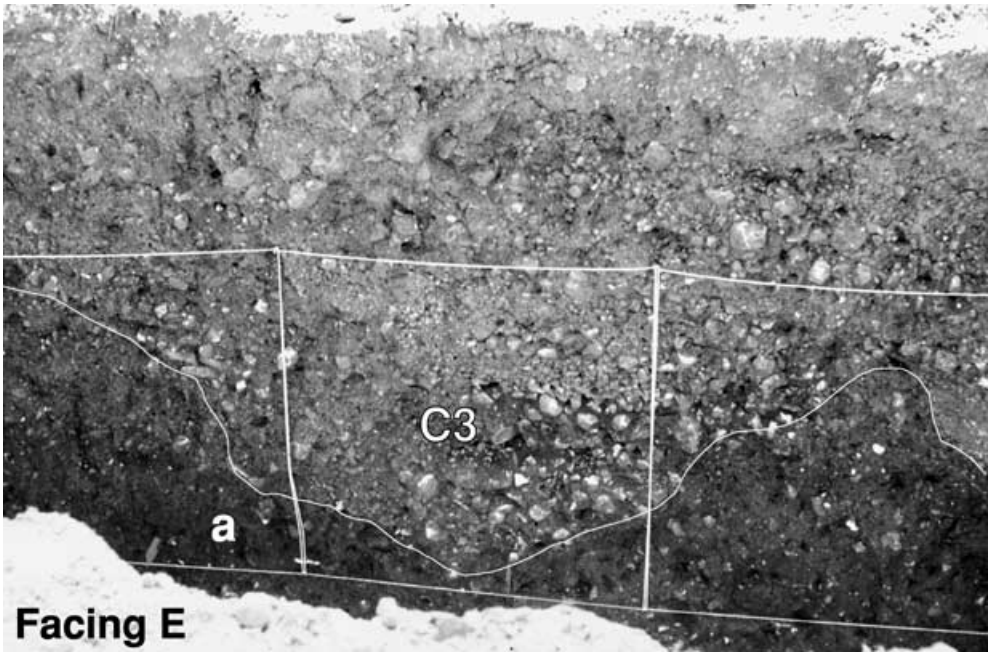

Figure 9. Photo of incised and filled channel exposed in Trench 2. Channel C3 is incised into the older alluvium (unit a) and filled with clast-supported cobble, gravel, and sand. White string grid has 1 m spacing.

graphitized carbon), a $\delta^{13}C$ measurement was not possible, hence an assumed value of 25 per cent was used. Other pre-Wedge 6 charcoal samples (also small) yielded high percentage modern values, and these probably reflect contamination. Radiocarbon dating of a complete (i.e. not truncated) exposure of this upper wedge in a small excavation to the north (see Fig. 3) demonstrated modern and >modern radiocarbon ages (Gomez *et al.* 2001). In summary, this uppermost colluvial wedge can be assigned a probable age 1650 AD to present.

Wedge 5 had a yellowish colour and consisted of large clasts with a white patina in a silty–sandy matrix. Charcoal from Wedge 5 yielded an age of 170 BC to 20 AD (2060 ± 30 BP). The down-slope stratigraphic equivalent is a fine sand/silt that can be traced across the shear zone abutting Wedge 6.

Wedge 4 rests directly beneath Wedge 5 and consists of small gravel and cobble-sized clasts in a silty-sandy matrix. Clasts of limestone and lacustrine sediment are present. Appropriate material for radiocarbon dating could not be found within this deposit. The sandy silt and gravel unit in the western end of the trench appears to be the down-slope stratigraphic equivalent of this unit.

Wedge 3 comprises limestone pebbles (centimetre size) and gravel in a sandy matrix. This unit is covered by the down-slope stratigraphic equivalent of Wedge 4 and truncates against the undifferentiated alluvium.

The oldest colluvium above the undifferentiated alluvium was Wedge 2. This deposit consisted of rounded pebbles and flat gravel in a stratified, reddish-brown matrix. Weakly developed soil structures were observed. Clasts consisted of limestone and lacustrine sediment. A bulk sediment sample from Wedge 2 yielded an age of 4050–3100 BC (4870 ± 160 BP).

Wedge 1 was identified in the base of the trench, within the undifferentiated alluvium. Well rounded pebbles and flat gravel of limestone and lacustrine sediment rest within a reddish-brown matrix. A bulk sample of the soil buried by this colluvial wedge was dated at 5730–5320 BC (6590 ± 120 BP).

In summary, the upper five distinct colluvial deposits post-date 5280 ± 230 BP. Stratigraphic relations demonstrate that all five post-alluvium colluvial wedges represent separate depositional episodes; i.e. there is a clear sequence of deposition and burial by successive colluvial deposits. The presence of weakly developed soil structures in the colluvial wedges suggests surface stability between distinct depositional events and argues against creation of the buried scarp by multiple events or fault creep. Hence, we interpret each colluvial wedge to post-date a separate palaeoseismic event that created each buried scarp.

2.5 Trench 2: abandoned channels

Trenches 2 and 3, parallel to the fault scarp, exposed the reddish-brown alluvium incised by channels (Fig. 9). Each channel was filled with moderately to well sorted, frequently clast supported gravel and occasional cobble, within a sandy matrix. This sedimentology indicates a moderately high-energy stream flow. Detrital charcoal collected from each of the channels provided age control of the filling sediments. In total, three channels, including the incision beneath the present-day drainage, were identified and correlated between the two trenches, with onlapping relationships demonstrating a consistent northward sense of younging (Fig. 10). For each channel, the magnitude of incision is greater in Trench 2 than in Trench 3, i.e. greater incision is found closer to the mouth of the drainage. In addition to stratigraphy, radiocarbon dating confirmed the correlation of channels between Trenches 2 and 3.

Channel C1 is filled by a fining upward sequence approximately 1 m thick. This is covered by about 1 m of recent alluvium that truncates and caps Channels C2 and C3. A charcoal fragment from the upper part of Channel C1 yields a calendar age of 600–780 AD (1354 ± 53 BP).

Channel C2 is very narrow and deeply incised (>2 m) into the older alluvium (unit a). During filling, small episodes of re-incision occurred, and the channel was capped by a thin veneer of alluvium

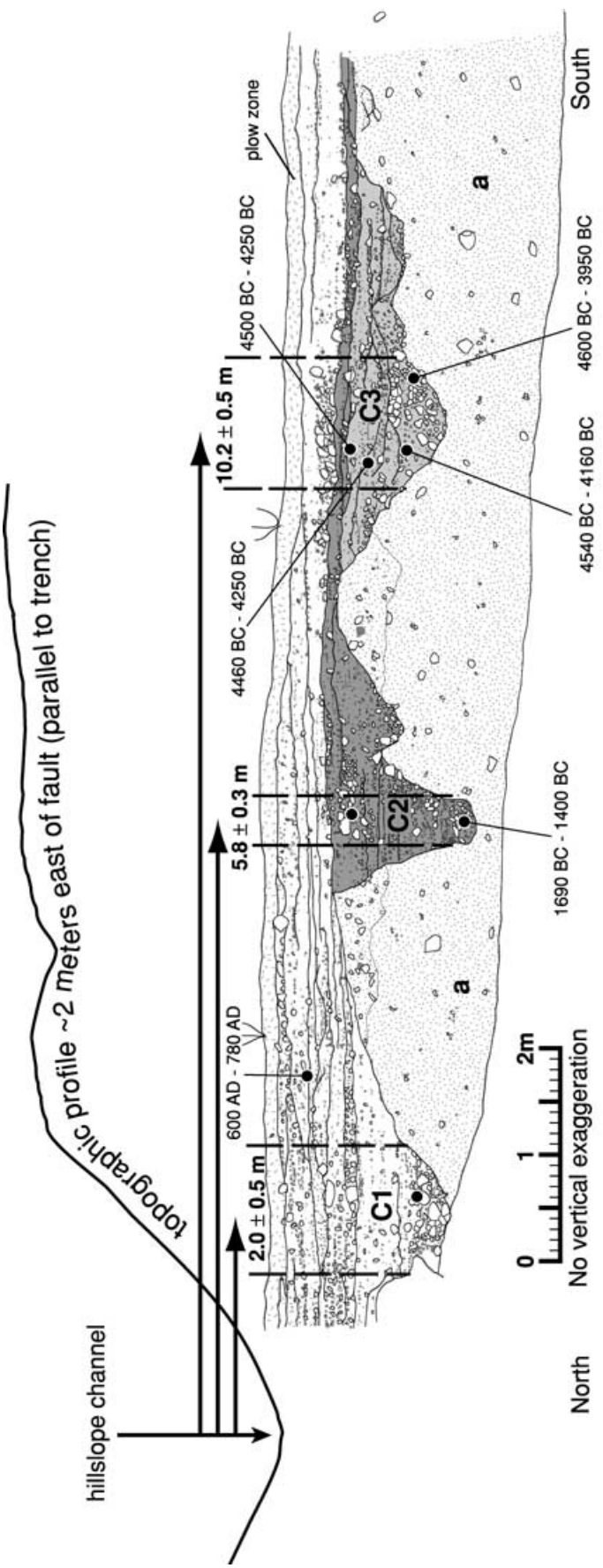

Figure 10. Trench log for the east wall of Trench 2. A sequence of three incised and filled channels is shown, with a northward sense of younging. Black discs denote the positions of samples for radiocarbon dating. The profile above the trench log depicts the hillslope channel morphology east of the fault zone. The relative positions of the channel mouth and the buried channels were mapped using a total station. Apparent offsets of the buried channels are shown.

that also caps Channel C3. The base of Channel C2 fill dates at 1690–1400 BC (3233 ± 57 BP).

Channel C3 depicts an initial incision followed by filling with minor episodes of entrenchment, meandering and widening of the original channel. Charcoal fragments from throughout the filling strata in Channel C3 yield statistically identical ages ($\chi^2 = 0.6 < 7.8$ (95 per cent), three degrees of freedom). Since these are from the same deposit, the ages and their Gaussian errors can be combined prior to calibration (Bronk Ramsey 1998) to yield a combined age of 5498 ± 46 BP for the fill. Recalling the 5280 ± 230 BP age from the top of the undifferentiated alluvium (unit a), which represents the incised surface, these ages are statistically very similar. This suggests that the cycle of incision and filling for Channel C3 was a relatively short-lived episode.

Channels 2 and 3 are exposed in both walls of trenches 2 and 3, and the positions of these channels depict linear traces approximately perpendicular to trenches 2 and 3 and to the fault trace (Fig. 5c). In addition, the active stream bed above incised Channel C1 also shows a very linear trace, aside from its abrupt deflection at the fault (Fig. 5c).

3 PALAEOSEISMIC INTERPRETATION: SLIP HISTORY OF THE SERGHAYA FAULT

3.1 Palaeoseismic chronology

Trench stratigraphy and associated chronological information allow the construction of a palaeoseismic record for the SFZ. The key palaeoseismic indicators in this study are the colluvial deposits exposed in Trench 1, along with the offsets of modern and buried stream channels. In Trench 1, Wedges 4–6 rest in depositional contact with the buried scarp located above shear zones. This suggests that each of these colluvial wedges corresponds to only one faulting event, i.e. that which produced the buried scarp. The sedimentary geometries of Wedges 1–3 suggest that they too each represent one depositional episode. Following the colluvial wedge model (McCalpin 1996), one colluvial wedge is deposited following each surface-rupturing earthquake. Stratigraphic relationships depict the colluvial wedges following a sequence, i.e. two wedges are not contemporaneous. Hence, we interpret six surface-rupturing earthquakes from this trench study (Fig. 11).

Combining the relative and absolute age control, a history of colluvial wedge deposition (each post-dating a palaeoseismic event) and channel scour-and-fill cycles can be assembled from the trench site. We interpret palaeoseismic events to pre-date colluvial wedges and to post-date channel incision/fill—if the fill post-dated an event, then it would be expected to comprise more chaotic colluvium derived from the channel wall, rather than the well-sorted sand and gravel that are observed. We also assume that the rapid incision/fill cycle of Channel C3 characterizes the incision and fill of Channels 1 and 2, although the geochronological data to test this assumption are lacking. We interpret these channel-scouring events to represent relatively short-lived climatic events within the increasing aridity during the Holocene.

Stratigraphic ties between Trenches 1 and 2 provide additional control on the relative timing of colluvial deposition and the scouring and filling of the buried channels. These stratigraphic ties are illustrated in the 3-D block diagram shown in Fig. 12. The upper fill of Channel C1 corresponds to the younger alluvial fan that locally buries the older alluvial apron. Stratigraphically, the remnant of Wedge 6 lies within this younger alluvial deposit. Another important stratigraphic tie is apparent between the upper part of the Channel C2 fill and the down-slope deposits interpreted to correspond to Wedge 4.

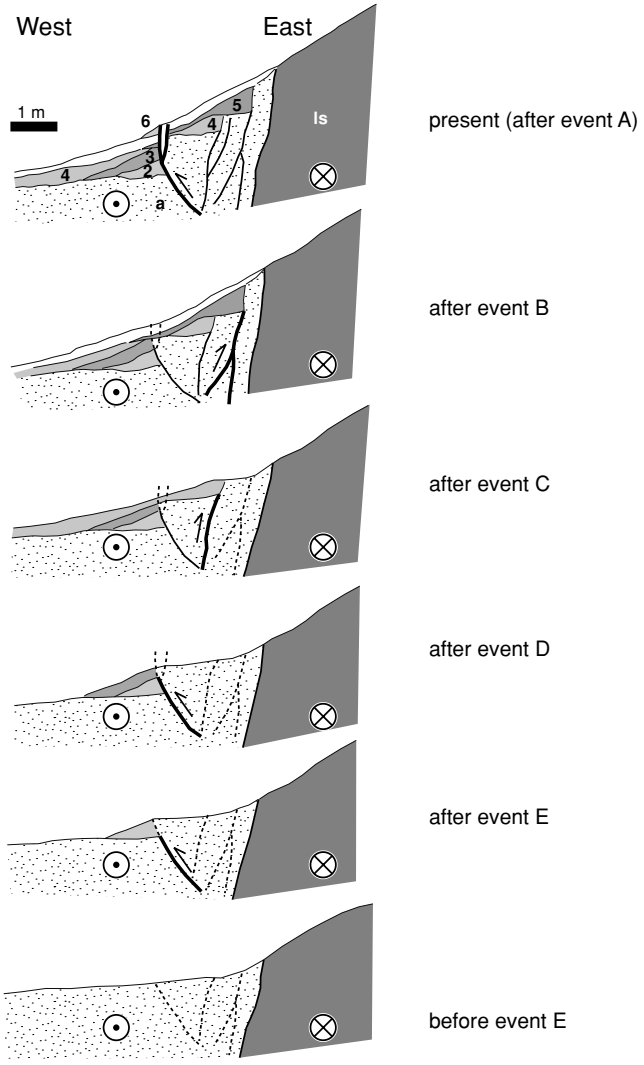

Figure 11. Cross-sections showing schematic reconstruction of the past five palaeoseismic events indicated in Trench 1. Numbers correspond to colluvial wedges 2–6. Bold lines depict the most recent fault splay in each stage; dashed lines denote restored faults. ls = lacustrine sediment; a = undifferentiated alluvium.

The channel incision/fill episodes and colluvial deposition events are summarized in Fig. 13, along with the interpreted palaeoseismic events, labelled A–F in order of increasing age. In total, five events are interpreted to post-date the older alluvium.

Remnants of Wedge 6 are within the younger alluvium and post-date the filling of Channel C1 (600–780 AD). Based on the remnants of Wedge 6, and the previous dating of the youngest colluvial wedge (Gomez *et al.* 2001), we interpret Wedge 6 as corresponding to an earthquake that occurred during the past two to three centuries (Event A), and this probably represents one of two well-documented, historical earthquakes that occurred in 1705 and 1759 (Table 1). Both earthquakes caused considerable damage in the AntiLebanon region. The 1705 earthquake caused considerable damage to Damascus (Poirier & Taher 1980). The earthquake of 1759 has been well documented (e.g. Ambraseys & Barazangi 1989) and most intensely affected towns in the western part of the AntiLebanon Mountains

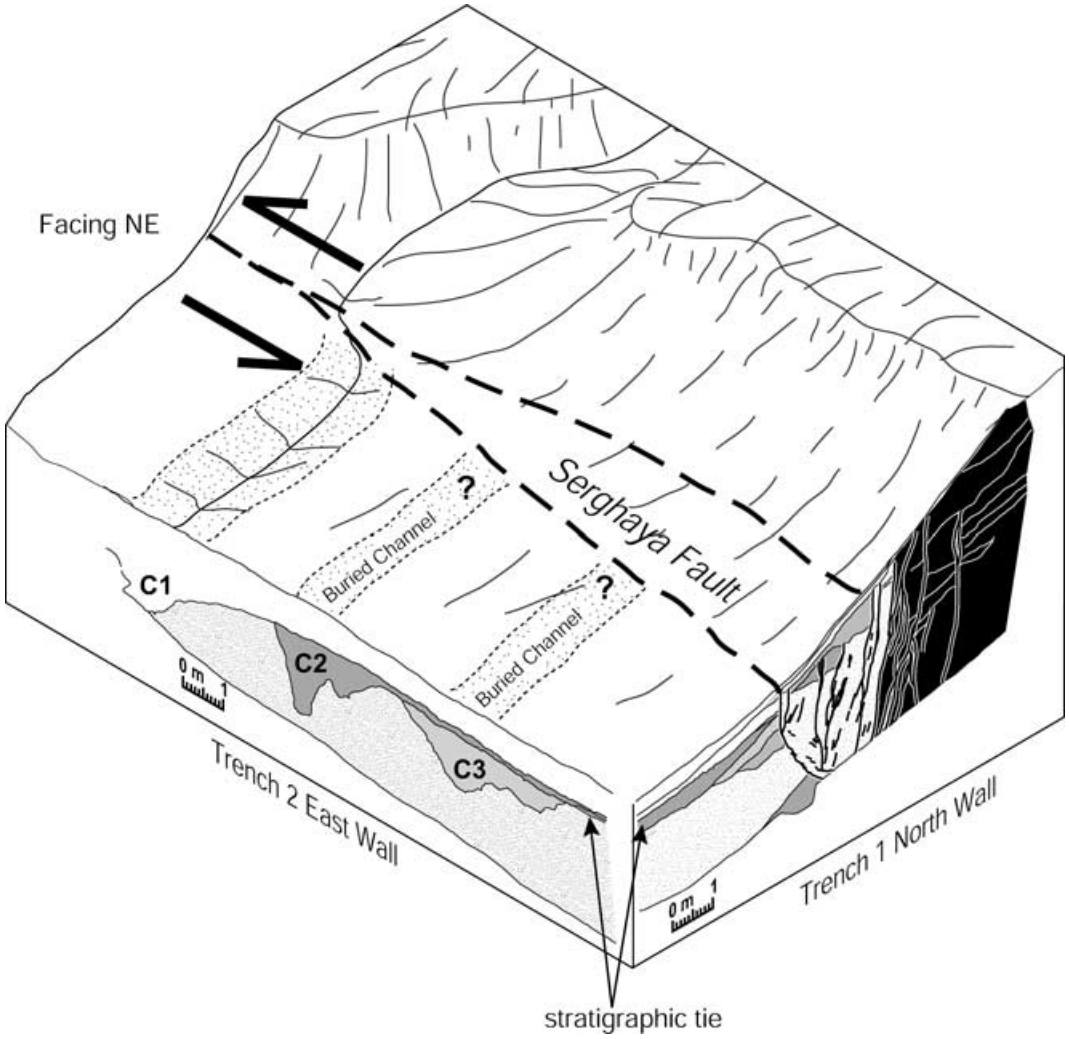

Figure 12. Schematic block diagram illustrating the 3-D relationships of the features exposed in the trenches. A stratigraphic tie between the filling deposit of Channel C2 with the down-slope equivalent of Wedge 4 can be observed.

and the Bekaa Valley. The macroseismic data suggest a magnitude of about 7.4 and up to 100 km of surface rupture. Reports of surface rupturing 'north of Baalbek' (Ambraseys & Barazangi 1989) are ambiguous concerning which side of the Bekaa Valley, and the surface rupture has not yet been identified in the field. From the dating in this trench alone, it is not possible to distinguish between these two events, as they occurred relatively close in time to one another during a time period for which radiocarbon age calibration is poorly controlled (e.g. Stuiver *et al.* 1998).

Wedges 5 is radiometrically constrained to pre-date the Channel C1 fill, and Wedge 4 is stratigraphically constrained to post-date the Channel C2 fill. Hence, two palaeoseismic events (events B and C) are interpreted as being between 170 BC–20 AD (Wedge 5) and 1690 BC–1400 BC (Channel C2). It may be possible that Wedge 5 (170 BC–20 AD) corresponds to a poorly documented earthquake that occurred in 198 BC. Although the reports for this earthquake come primarily from Sidon on the coast of present-day Lebanon, the onshore location of this earthquake is suggested by the report that a town inland was 'engulfed' by the earthquake (Ambraseys & White 1997). However, such an interpretation is speculative until the other possible fault branches (e.g. Yammouneh and Roum faults) have been studied and discounted as possible sources.

Wedge 2 is radiometrically constrained to post-date the Channel C3 fill, and we believe that Wedge 3 also pre-dates Channel C2. Consequently, two additional palaeoseismic events (events D and E) are interpreted between 1690–1400 BC (Channel C2) and 4460–4250 BC (radiocarbon dates combined before calibration) (Channel C3). Event E can be constrained to post-date the Channel C3 fill (4460–4250 BC) and pre-date Wedge 2 (4050–3250 BC).

The oldest palaeoseismic event in the trench, represented by Wedge 1, pre-dates the bulk sample from the upper part of the undifferentiated alluvium (unit a) and postdates the buried soil below Wedge 1 (5730– 5320 BC). Hence, this palaeoseismic event probably occurred some time between 5600 and 4400 BC (at the 2σ confidence limits).

3.2 Displacements

The buried channels exposed in Trenches 2 and 3 serve as piercing points of different ages and provide a means of determining a Holocene slip rate for the Serghaya fault. These channels depict quasi-linear traces and a northward sense of younging consistent with left-lateral transport of the downstream reaches from the mouth of the drainage. Although it is not possible to date the incision

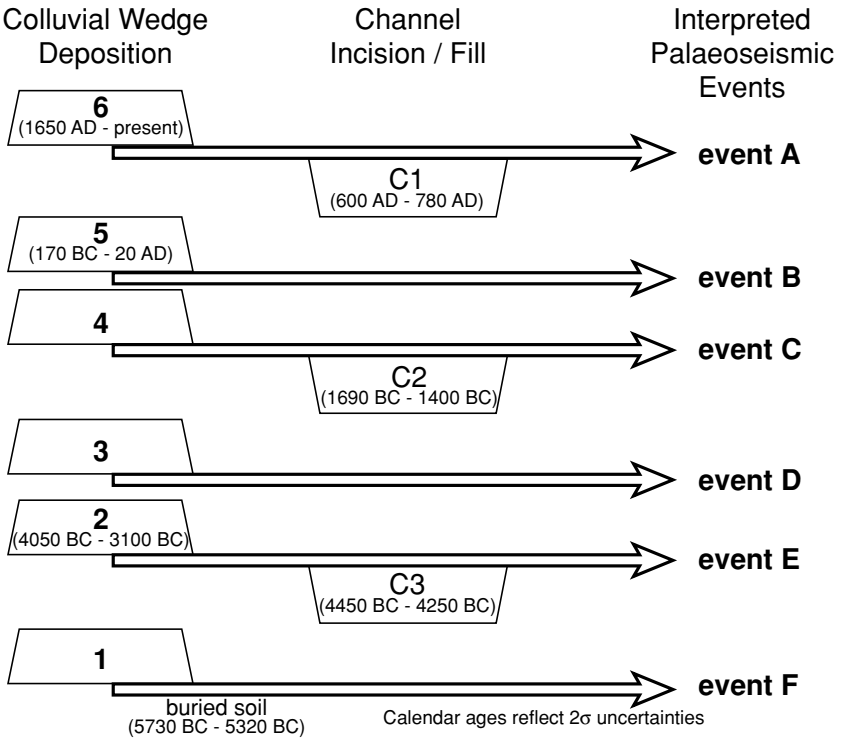

Figure 13. Summary of events observed in the trenches and the interpreted palaeoseismic history of the Serghaya fault. Colluvial wedge deposits post-date palaeoseismic events. Stratigraphic ties provide additional constraint on the relative timing of events. Ages represent calendar corrected radiocarbon ages for given features (2σ uncertainties provided).

directly, the rapid cycle of incision and fill in Channel C3 based on the radiocarbon dates may characterize Channels 1 and 2, as well.

The buried channels correspond to episodic entrenchment of the alluvial apron, probably resulting from infrequent major storms in this semi-arid environment. The fill, consisting of sorted sand and gravel, is consistent with water-lain transport. Short-lived cycles of channel incision and subsequent filling are typical in arroyo development in the semi-arid regions of western North America where incision results from increased stream power, probably due to a short-lived, but relatively intense flow in the channel (Bull 1997). A concentrated flow (required to erode the channel) exiting the mouth of the drainage would probably follow a linear flow path, and this interpretation is consistent with the quasi-linear channel traces observed in the trenches and the present-day drainage. Hence, it seems reasonable to project the linear traces of the channels uphill to the fault zone in order to estimate the amount of displacement for each channel. Linear channels are also suggested by the exposures of Channels C2 and C3 in both walls of trenches 2 and 3 (Fig. 5c). The channel mouth morphology and its position relative to the trench wall were mapped with a total station. The incised widths are estimated based on the bottom 50 cm of each channel, and displacements of 2.0 ± 0.5, 5.8 ± 0.3 and 10.2 ± 0.5 m are estimated from the channels (see Figs 10 and 5c).

A plot of displacement versus age of the channel fill depicts an average slip rate of 1.4 ± 0.2 mm yr^{-1} (Fig. 14). This slope was determined by linear regression of the displaced channel data with 2σ uncertainties. Although the sand and gravel in Channel C1 is dated to 680–780 AD, the timing of the displacement of this channel is constrained by historical records to post-date the channel by more than 1000 yr (following our interpretation of an 18th century earthquake on the Serghaya fault). Hence, the slope of the line in Fig. 14 was determined using the timing of displacement of C1 in the 18th century.

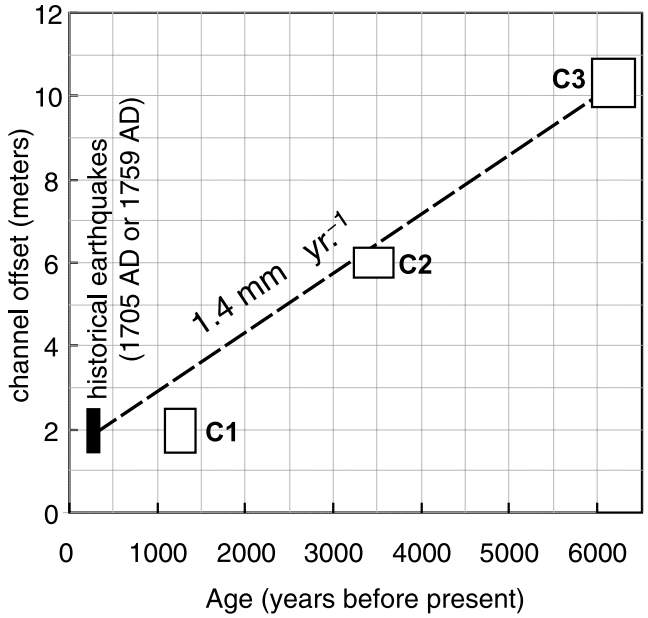

Figure 14. Plot of offset versus age for buried channels. The 2 m displacement of the youngest channel corresponds to a historically documented earthquake in the early or mid 18th century. The slope of the linear fit is the average Holocene slip rate for the Serghaya fault.

The displacements and event histories tie together as follows: (1) 2 m of displacement associated with event A (the historical event

and the small stream deflection); (2) ∼4 m of displacement associated with events B and C; and (3) ∼4 m of displacement associated with events D and E. The displacement for the last event appears to be roughly constant over the 6–7 km spanning the southern Zebadani Valley, as suggested by the minimum drainage deflections (Fig. 3). The individual slip for events B, C, D and E cannot be estimated. However, each pair of events B/C (corresponding to the displacement of channel C2) and D/E (corresponding to the offset of channel C3) demonstrates an average left-lateral slip of ∼2 m per event. Hence, this section of the Serghaya fault might be characterized by similar slip in each of the last five paleoseismic events. Similar slip per event is also suggested by the similar thickness of colluvial wedges 1–5 (30–50 cm), although, as discussed by McCalpin (1996), colluvial wedge thickness is not always and uniquely related to uplift.

Constant slip for repeated earthquakes is also inferred on the southern section of the DSFS by Klinger *et al.* (2000b), as well as on strike-slip faults in California (e.g. Lindvall *et al.* 1989; Sieh 1996; Rubin & Sieh 1997). This co-seismic slip behaviour is typical for both the uniform slip (Sieh 1981) and characteristic earthquake (Schwartz & Coppersmith 1984) models of earthquake repetition. However, in order to discriminate between these two types of earthquake behaviour, additional locations along the 125 km long Serghaya fault need to be studied. For example, the uniform slip model involves a constant slip rate along the fault and frequent moderate earthquakes to compensate for along-strike variations in slip per event at a given location; the characteristic earthquake model allows a variable slip rate along the fault and infrequent moderate earthquakes. It should also be noted that other sections of the DSFS demonstrate variable displacement for repeated earthquakes (e.g. Ellenblum *et al.* 1998).

Applying published scaling laws relating slip to moment magnitude (e.g. Wells & Coppersmith 1994), 2 m of slip corresponds to an earthquake of $M_w \sim 7$–7.2. On average, this portion of the Serghaya fault has experienced one such event every ∼1300 yr. Although in many cases, the time brackets on the individual palaeoseismic events are not well resolved, the available timing constraints are consistent with this mean return period. However, the actual recurrence intervals may vary significantly. For example, Wedge 2, which post-dates the penultimate event, is dated as 170 BC–20 AD, whereas the last event occurred in the early to mid 18th century. This implies that at least 1700–1900 yr elapsed between these two events.

A time-predictable earthquake model uses the displacement of the last event and the slip rate to predict the time to the next earthquake, assuming that the fault fails at a critical stress level (Shimazaki & Nakata 1980). In the context of such an earthquake recurrence model, the slip rate and the palaeoseismic history (2.0–2.5 m of slip in the last earthquake with a slip rate of 1.4 mm yr^{-1}) suggest that there is probably not a slip deficit on this portion of the Serghaya fault. However, this is only a preliminary interpretation based on this one palaeoseismic investigation. Regardless of the lack of a slip deficit, consideration should be given to possible stress interactions between the Serghaya fault and the nearby Yammouneh or Roum faults.

4 TECTONIC IMPLICATIONS

Active strike-slip movement of the Serghaya fault contrasts with suggestions that strike-slip faulting within the restraining bend and northwards have been rendered inactive as a result of an evolving regional stress field in the eastern Mediterranean region (e.g. Butler *et al.* 1997). A recent plate model for the Arabian and African plates based on GPS measurements (McClusky *et al.* 2003) predicts the total motion of the Arabian plate relative to the African plate at this latitude to be ∼6.8 mm yr^{-1} with an azimuth of about N25W, i.e. 45° to the azimuth of the restraining bend. Primarily left-lateral slip on the Serghaya fault, striking N20E, suggests a regional partitioning of strain.

One simple geometrical model of strain partitioning in the restraining bend along the Dead Sea fault system is illustrated schematically in Fig. 15(a). In this model, the plate motion is decomposed into 4.8 mm yr^{-1} of strike-slip along faults striking N20E in the restraining bend, as well as a similar magnitude of shortening perpendicular to the faults (Fig. 15a). In this case, the 1.4 ±

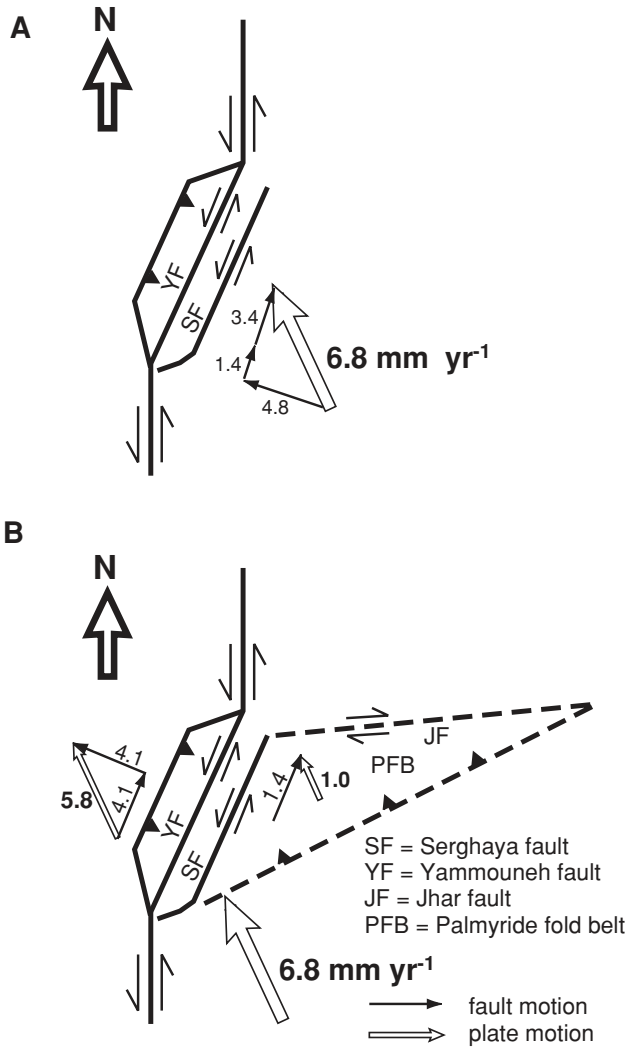

Figure 15. Two simplified geometrical models for the restraining bend of the Dead Sea fault system and the role of the Serghaya fault. Predicted plate motion is based on the GPS-derived regional plate model of McClusky *et al.* (2003, in press). (a) Decomposing the predicted plate motion into N20E strike-slip fault and orthogonal shortening, the 1.4 mm yr^{-1} of slip on the Serghaya fault accounts for ∼30 per cent of the expected strike-slip movement on faults striking N20E. The orthogonal shortening would be accommodated in the Mt Lebanon and/or AntiLebanon Mountains. (b) An alternative model in which the Serghaya fault acts as an oblique back-stop behind the Palmyride fold belt and contributes to internal deformation of the Arabian plate. The remaining portion of Arabian–African plate motion may then be composed into strike-slip movement (N20E faults) and orthogonal shortening.

0.2 mm yr^{-1} of slip on the Serghaya fault only accounts for ~30 per cent of total predicted strike-slip motion. Consequently, this implies that other strike-slip faults in the restraining bend, such as the Yammouneh fault, should be active in order to accommodate the remaining plate motion.

However, the Serghaya fault does not appear to reconnect with the transform (Figs 1 and 2), suggesting a slightly more complicated fault model. One possibility might involve the Serghaya fault acting as an oblique 'back-stop' for active shortening within the adjacent Palmyride fold belt, perhaps along with the right-lateral Jhar fault north of the Palmyrides (Fig. 15b). In this case, the 1.4 ± 0.2 mm yr^{-1} of slip on the Serghaya fault may be used to infer from the geometry that NNW shortening in the Palmyrides accommodates approximately 1 mm yr^{-1} of the relative plate motion. The remaining 5.8 mm yr^{-1} of plate motion could be decomposed into 4.1 mm yr^{-1} of strike-slip on N20E strike-slip faults (e.g. the Yammouneh fault), and a similar amount of shortening perpendicular to these faults.

Regardless of the general tectonic model for the restraining bend, the Serghaya fault seems insufficient to account for all predicted plate motion. Hence, multiple strike-slip faults imply more complicated scenarios for earthquake hazard assessments.

As noted by previous workers this structural configuration bears similarity to the 'Big Bend' of the San Andreas fault system in southern California (e.g. Chaimov *et al.* 1990), which comprises several active fault branches, including both reverse and strike-slip faults. In addition, internal deformation of the North American Plate is also significant—although the major component of plate motion is accommodated by the San Andreas fault, studies have demonstrated that the Eastern California Shear Zone and the Basin and Range (e.g. Dokka & Travis 1990; Dickinson & Wernicke 1997) accommodate significant components of the total plate motion.

5 CONCLUSIONS

This study provides an initial view of the earthquake behaviour and active fault kinematics for the Serghaya fault, and these results depict recent tectonic activity that is not readily apparent in the instrumentally recorded seismicity alone. The Serghaya fault is active, and the total fault length and 2–2.5 m displacements, combined with historical seismicity, suggest that the fault may be capable of generating large ($M \sim 7$) earthquakes. This study also provides a first view of the earthquake recurrence history along the Serghaya fault. The results suggest a slip rate of about 1.4 mm yr^{-1}, with an average of approximately 2 m of slip per event at this location and a mean repeat time of about 1300 yr. However, the age control from the colluvial deposits is relatively limited for placing tight limits on the timing of past events, although these can be identified with loose constraints. Additional studies are needed to illuminate any fault-wide behaviour, such as fault segmentation, to distinguish between models of fault behaviour such as the characteristic earthquake and uniform slip models. Understanding the extent and magnitude of past ruptures can also provide critical input for modelling static stress interactions on nearby faults that can increase or decrease the probabilities of subsequent earthquakes.

Although this study has documented the inferred effects of large, surface-rupturing earthquakes on the Serghaya fault, moderate earthquakes ($M \sim 5$–6) are also a concern for seismic hazard assessments. The recurrence of moderate earthquakes can be difficult to assess using palaeoseismic techniques—moderate earthquakes do not always produce a surface rupture, and when they do, slip is small and of limited spatial extent. However, moderate earthquakes, if relatively frequent, can also present a considerable hazard if the epicentres are located near cities such as Damascus or Beirut. Eventual distinction of different models for earthquake behaviour, such as the characteristic earthquake (infrequent moderate earthquakes) versus uniform slip (relatively frequent moderate earthquakes) models, will assist in assessing the level of hazard posed by moderate earthquakes.

The results of this study demonstrate that the Serghaya fault is a significant element of this portion of the Arabian–African plate boundary. When placed in the context of Arabian–African relative plate motions, the slip rate and fault kinematics suggest that other structures must also be active within the restraining bend in order to accommodate the expected plate motion. Ongoing GPS observations and future geological studies should help clarify the kinematics of the restraining bend and the means by which it connects the two simpler sections of the Dead Sea fault system. This will ultimately contribute to a better understanding of the structural behaviour and evolution of continental transform systems.

ACKNOWLEDGMENTS

The field investigation presented here benefited from significant logistical support provided by the Higher Institute of Applied Sciences and Technology (HIAST). G. Brew, Y. Radwan, I. Layous, H. Al-Najar, M. Daoud, C. Tabet and M. Khawlie contributed additional assistance to the trench study. D. Seber provided helpful comments in the development of this manuscript. The late Dr G. Bock provided constructive comments and support as the editor of GJI. We also thank S. Marco and A. Agnon as official reviewers of GJI for their helpful suggestions in revising the manuscript. Radiocarbon dating by PRIME Laboratory (Purdue University) was provided through seed project J019. This research was partially supported by NSF grants EAR-0106238 and NSF INT-9810510. MM was supported by CNRS-UMR 7516.

REFERENCES

Al Ghazzi, R., 1982. Les failles libano-syriennes; implications tectoniques et sismiques a l'aide des donnees Landsat, *Proc. of the International Symp. of Commission VII of the International Society of Photogrammetry and Remote Sensing,* pp. 562–565, Groupement Develop. Teledetection Aerospatiale. Toulouse, France.

Ambraseys, N.N. & Barazangi, M., 1989. The 1759 Earthquake in the Bekaa Valley: implications for earthquake hazard assessment in the Eastern Mediterranean region, *J. geophys. Res.,* **94,** 4007–4013.

Ambraseys, N.N. & Jackson, J.A., 1998. Faulting associated with historical and recent earthquakes in the Eastern Mediterranean region, *Geophys. J. Int.,* **133,** 390–406.

Ambraseys, N.N. & White, D., 1997. The seismicity of the eastern Mediterranean region 550–1 BC: a re-appraisal, *J. Earthquake Eng.,* **1,** 603–632.

Ambraseys, N.N., Melville, C.P. & Adams, R.D., 1994. *The Seismicity of Egypt, Arabia and the Red Sea; a Historical Review,* p. 181, Cambridge University Press, Cambridge.

Amiran, D.H.K., Arieh, E. & Turcotte, T., 1994. Earthquakes in Israel and adjacent areas: macroseismic observations since 100 B.C.E., *Israel expl. J.,* **44,** 260–305.

Ben Menahem, A., Nur, A. & Vered, M., 1976. Tectonics, seismicity and structure of the Afro-Eurasian Junction; the breaking of an incoherent plate, *Phys. Earth planet. Inter.,* **12,** 1–50.

Beydoun, Z.R., 1999. Evolution and development of the Levant (Dead Sea Rift) Transform System: a historical-chronological review of a structural controversy, in *Continental Tectonics,* pp. 239–255, eds MacNiocaill, C. & Ryan, P.D., Geological Society of London, London.

Biasi, G. & Weldon, R., 1994. Quantitative refinement of C-14 distributions, *Quat. Res.,* **41,** 1–18.

Brew, G., Barazangi, M., Al-Maleh, A.K. & Sawaf, T., 2001. Tectonic and geologic evolution of Syria, *GeoArabia,* **6,** 573–616.

Bronk Ramsey, C., 1998. Probability and dating, *Radiocarbon,* **40,** 461–474.

Bull, W., 1997. Discontinuous ephemeral streams, *Geomorphology,* **19,** 227–276.

Butler, R.W.H., Spencer, S. & Griffiths, H.M., 1997. Transcurrent fault activity on the Dead Sea Transform in Lebanon and its implications for plate tectonics and seismic hazard, *J. geol. Soc. Lond.,* **154,** 757–760.

Chaimov, T.A., Barazangi, M., Al-Saad, D., Sawaf, T. & Gebran, A., 1990. Crustal shortening in the Palmyride fold belt, Syria, and implications for movement along the Dead Sea fault system, *Tectonics,* **9,** 1369–1386.

Darawcheh, R., Sbeinati, M.R., Margottini, C. & Paolini, S., 2000. The 9 July 551 AD Beirut earthquake, eastern Mediterranean region, *J. Earthquake Eng.,* **4,** 403–414.

Dickinson, W.R. & Wernicke, B.P., 1997. Reconciliation of San Andreas slip discrepancy by a combination of interior Basin and Range extension and transrotation near the coast, *Geology,* **25,** 663–665.

Dokka, R.K. & Travis, C.J., 1990. Role of the Eastern California shear zone in accommodating Pacific–North American Plate motion, *Geophys. Res. Lett.,* **17,** 1323–1326.

Dubertret, L., 1955. Carte Geologique du Liban, Lebanese Ministry of Public Works, 1:200 000.

Dubertret, L., 1962. Carte Geologique du Liban, Syrie et bordure des pays voisins, Museum National D'Histoire Naturelle, Paris, 1:1,000 000.

El-Isa, Z.H. & Mustafa, H., 1986. Earthquake deformations in the Lisan deposits and seismotectonic implications, *Geophys. J. R. astr. Soc.,* **86,** 413–424.

Ellenblum, R., Marco, S., Agnon, A., Rockwell, T. & Boas, A., 1998. Crusader castle torn apart by earthquake at dawn, 20 May 1202, *Geology,* **26,** 303–306.

Freund, R., Zak, I., Goldberg, M., Weissbrod, T. & Derin, B., 1970. The shear along the Dead Sea Rift, *Phil. Trans. R. Soc. Lond.,* A., **267,** 107–310.

Garfunkel, Z., Zak, I. & Freund, R., 1981. Active faulting in the Dead Sea rift, *Tectonophysics,* **80,** 1–26.

Girdler, R.W., 1990. The Dead Sea transform fault system, *Tectonophysics,* **180,** 1–13.

Gomez, F. *et al.*, 2001. Coseismic displacements along the Serghaya fault: an active branch of the Dead Sea fault system in Syria and Lebanon, *J. geol. Soc. Lond.,* **158,** 405–408.

Heimann, A. & Ron, H., 1993. Geometric changes of plate boundaries along part of the northern Dead Sea Transform; geochronologic and paleomagnetic evidence, *Tectonics,* **12,** 477–491.

Hempton, M.R., 1987. Consrtaints on Arbaian plate motion and extensional history of the Red Sea, *Tectonics,* **6,** 687–705.

Jackson, J. & McKenzie, D., 1988. The relationship between plate motions and seismic moment tensors, and rates of active deformation in the Mediterranean and Middle East, *Geophys. J.,* **93,** 45–73.

Jestin, F., Huchon, P. & Gaulier, J.M., 1994. The Somalia plate and the Eastern Africa Rift System: present-day kinematics, *Geophys. J. Int.,* **116,** 637–654.

Joffe, S. & Garfunkel, Z., 1987. Plate kinematics of the circum Red Sea—a re-evaluation, *Tectonophysics,* **141,** 5–22.

Ken-Tor, R., Agnon, A., Enzel, Y., Stein, M., Marco, S. & Negendank, J.F.W., 2001. High-resolution geological record of historic earthquakes in the Dead Sea basin, *J. geophys. Res.,* **106,** 2221–2234.

Klinger, Y., Rivera, L., Haessler, H. & Maurin, J.-C., 1999. Active faulting in the Gulf of Aqaba: new knowledge from the M_w 7.3 earthquake of 22 November 1995, *Bull. seism. Soc. Am.,* **89,** 1025–1036.

Klinger, Y., Avouac, J.P., Abou Karaki, N., Dorbath, L., Bourles, L. & Reys, J., 2000a. Slip rate on the Dead Sea transform fault in the northern Araba Valley (Jordan), *Geophys. J. Int.,* **142,** 755–768.

Klinger, Y., Avouac, J.P., Dorbath, L., Abou Karaki, N. & Tisnerat, N., 2000b. Seismic behaviour of the Dead Sea fault along the Araba valley, Jordan, *Geophys. J. Int.,* **142,** 769–782.

Lindvall, S.C., Rockwell, T.K. & Hudnut, K.W., 1989. Evidence for prehistoric earthquakes on the Superstition Hills fault from offset geomorphic features, *Bull. seism. Soc. Am.,* **79,** 342–361.

Marco, S., Stein, M., Agnon, A. & Ron, H., 1996. Long-term earthquake clustering: A 50 000 year paleoseismic record in the Dead Sea Graben, *J. geophys. Res.,* **101,** 6179–6191.

McCalpin, J.P., 1996. *Paleoseismology,* p. 588, Academic Press, San Diego, CA.

McClusky, S. *et al.*, 2000. GPS constraints on plate motion and deformation in the eastern Mediterranean: Implications for plate dynamics, *J. geophys. Res.,* **105,** 5695–5719.

McClusky, S., Reilinger, R., Mahmoud, S., Ben Sari, D. & Tealeb, A., 2003. GPS Constraints on Africa (Nubia) and Arabia plate motions, *Geophys. J. Int.,* in press.

Meghraoui, M. *et al.*, 2003. Evidence for 830 years of seismic quiescence from paleoseismology, archeoseismology and historical seismicity along the Dead Sea Fault in Syria, *Earth planet. Sci. Lett.,* in press.

Mohamad, R., Darkal, A.N., Seber, D., Sandvol, E., Gomez, F. & Barazangi, M., 2000. Remote earthquake triggering along the Dead Sea fault system following the 1995 Gulf of Aqaba earthquake ($M_s = 7.3$), *Seism. Res. Lett.,* **71,** 47–52.

Pinar, A. & Turkelli, N., 1997. Source inversion of the 1993 and 1995 Gulf of Aqaba earthquakes, *Tectonophysics,* **283,** 279–288.

Poirier, J.P. & Taher, M.A., 1980. Historical seismicity in the Near and Middle East, North Africa, and Spain from Arabic documents (VIIth–XVIIIth century), *Bull. seism. Soc. Am.,* **70,** 2185–2201.

Quennell, A.M., 1984. The Western Arabia rift system, in *The Geological Evolution of the Eastern Mediterranean,* pp. 775–788, eds Dixon, J.E. & Robertson, A.H.F., Blackwell, Oxford.

Ron, H., 1987. Deformation along the Yammuneh, the restraining bend of the Dead Sea transform: paleomagnetic data and kinematic implications, *Tectonics,* **6,** 653–666.

Rubin, C.M. & Sieh, K., 1997. Long dormancy, low slip rate, and similar slip-per-event for the Emerson fault, eastern California shear zone, *J. geophys. Res.,* **102,** 15 319–15 333.

Sbeinati, M.R., Darawcheh, R. & Mouty, M., 2003. Seismic data for siting and site-revalidation of nuclear facility, Part 1: Catalog of historical earthquakes in and around Syria, *Ann. Geofis.,* in press.

Schwartz, D.P. & Coppersmith, K.J., 1984. Fault behavior and characteristic earthquakes: examples from the Wasatch and San Andreas Fault zones, *J. geophys. Res.,* **89,** 5681–5698.

Shimazaki, K. & Nakata, T., 1980. Time-predictable recurrence model for large earthquakes, *Geophys. Res. Lett.,* **7,** 279–282.

Sieh, K., 1981. A review of geological evidence for recurrence times of large earthquakes, in *Earthquake Prediction, an International Review,* pp. 181–207, eds Simpson, D.W. & Richards, P.G., Maurice Ewing Series, Volume 4, American Geophysical Union, Washington, DC.

Sieh, K., 1996. The repetition of large-earthquakes ruptures, *Proc. Natl Acad. Sci., USA,* **93,** 3764–3771.

Stein, R.S., Barka, A.A. & Dieterich, J.H., 1997. Progressive failure on the North Anatolian fault since 1939 by earthquake stress triggering, *Geophys. J. Int.,* **128,** 594–604.

Stuiver, M. *et al.*, 1998. INTCAL98 Radiocarbon Age Calibration, 24 000–0 cal BP, *Radiocarbon,* **40,** 1041–1083.

Walley, C.D., 1988. A braided strike-slip model for the northern continuation of the Dead Sea Fault and its implications for Levantine tectonics, *Tectonophysics,* **145,** 63–72.

Wells, D.L. & Coppersmith, K.J., 1994. New empirical relationships among magnitude, rupture length, rupture width, rupture area, and surface displacement, *Bull. seism. Soc. Am.,* **84,** 974–1002.

Westaway, R., 1994. Present-day kinematics of the Middle East and eastern Mediterranean, *J. geophys. Res.,* **99,** 12 071–12 090.

Zilberman, E., Amit, R., Heimann, A. & Porat, N., 2000. Changes in Holocene paleoseismic activity in the Hula pull-apart basin, Dead Sea Rift, northern Israel, *Tectonophysics,* **321,** 237–252.